

**SOURCE PHYSICS EXPERIMENT: RESEARCH IN SUPPORT OF VERIFICATION AND
NONPROLIFERATION**

Wendee M. Brunish, Christopher R. Bradley, Esteban Rougier, Howard J. Patton, David Coblenz,
David W. Steedman, Aviva J. Sussman, and Earl. E. Knight

Los Alamos National Laboratory

Sponsored by the National Nuclear Security Administration

Award No. DE-AC52-06NA25396/LA10-SOURCE-NDD02

ABSTRACT

The Source Physics Experiment (SPE-N) was designed to provide a carefully controlled seismic and strong motion data set from buried explosions at the Nevada National Security Site (NNSS). The first experiment in a series (SPE1) was conducted in May of this year. It consisted of a 100 kg high explosive stemmed for coupling at 180 feet below the surface. In preparation for this experiment, predictive hydrodynamic calculations were performed, strong ground motion free-field and surface gauges were fielded, and a dense network of seismometers and some complimentary infrasound sensors were deployed. The data return for a majority of these sensors was excellent. This paper reports on a finite element analysis of the observable effects of an explosion in realistic earth material with particular focus on predicted and observed strong ground motion patterns. The model correctly incorporates the near-field cavity dynamics, energy deposition partitioned into internal (heat and plastic strain) and kinetic (e.g., radiated seismic) energy, giving more confidence in predicted free-field displacement/velocities and measured attenuation of the free-field peak velocity with distance. The degree of source asymmetry is studied with predictions of the hydrodynamic calculations for close-in free-field particle velocities. We present progress in improving our near-source modeling and predictive capabilities. A number of material test are presented on the granodiorite for both intact and weathered/damaged rock samples. These were used to improve our material model for the near-source environment. Additionally, a detailed 3D geologic framework model was created to represent the complex heterogeneities in the near-source environment (topography, faults, lithology, saturation and weathering). The improved material model was used in a set of 2D axially symmetric and a set of 3D simulations developed for simulating the Source Physics Experiment site. The site is dissected by two prominent faults. These faults have proven to control the radial asymmetry of the near field ground motion. Comparisons to the data provide ample information to study dry and water-saturated fractures, local lithology and topography on the radiated seismic wavefield.

Spallation on SPE1 is predicted well by an empirical scaling relationship developed for nuclear explosions with nominal scaled depths of burial ($\sim 120 \text{ m/kt}^{1/3}$). This fact is astonishing considering that SPE1 is very over-buried, $940 \text{ m/kt}^{1/3}$. This result is probably due to compensating effects of a low-porosity granite medium and a water table reaching almost to the free surface on Climax Stock. Nuclear tests on which the empirical relationship was based were overlain with ~ 640 meters of tuff with varying degrees of porosity which absorbs energy carried by shock waves. Estimates of bulk wave speeds in a weathered layer and in the basement rock where SPE1 was emplaced were obtained from P travel times and Rg dispersion curves. These speeds are considerably lower than those determined from core samples, illustrating the contrast typical of length scales of the measurements (100s of meters versus 0.1 meters).

Note: The Source Physics Experiments at the Nevada Nuclear Security Site (SPE-N) in 2011 should not be confused with the 2003 Source Phenomenology Experiments conducted in Arizona (SPE-A) (Yang and Bonner, 2009)

Report Documentation Page

Form Approved
OMB No. 0704-0188

Public reporting burden for the collection of information is estimated to average 1 hour per response, including the time for reviewing instructions, searching existing data sources, gathering and maintaining the data needed, and completing and reviewing the collection of information. Send comments regarding this burden estimate or any other aspect of this collection of information, including suggestions for reducing this burden, to Washington Headquarters Services, Directorate for Information Operations and Reports, 1215 Jefferson Davis Highway, Suite 1204, Arlington VA 22202-4302. Respondents should be aware that notwithstanding any other provision of law, no person shall be subject to a penalty for failing to comply with a collection of information if it does not display a currently valid OMB control number.

1. REPORT DATE

SEP 2011

2. REPORT TYPE

3. DATES COVERED

00-00-2011 to 00-00-2011

4. TITLE AND SUBTITLE

Source Physics Experiment: Research in Support of Verification and Nonproliferation

5a. CONTRACT NUMBER

5b. GRANT NUMBER

5c. PROGRAM ELEMENT NUMBER

6. AUTHOR(S)

5d. PROJECT NUMBER

5e. TASK NUMBER

5f. WORK UNIT NUMBER

7. PERFORMING ORGANIZATION NAME(S) AND ADDRESS(ES)

Los Alamos National Laboratory, P.O. Box 1663, Los Alamos, NM, 87545

8. PERFORMING ORGANIZATION REPORT NUMBER

9. SPONSORING/MONITORING AGENCY NAME(S) AND ADDRESS(ES)

10. SPONSOR/MONITOR'S ACRONYM(S)

11. SPONSOR/MONITOR'S REPORT NUMBER(S)

12. DISTRIBUTION/AVAILABILITY STATEMENT

Approved for public release; distribution unlimited

13. SUPPLEMENTARY NOTES

Published in the Proceedings of the 2011 Monitoring Research Review - Ground-Based Nuclear Explosion Monitoring Technologies, 13-15 September 2011, Tucson, AZ. Volume I. Sponsored by the Air Force Research Laboratory (AFRL) and the National Nuclear Security Administration (NNSA). U.S. Government or Federal Rights License

14. ABSTRACT

The Source Physics Experiment (SPE-N) was designed to provide a carefully controlled seismic and strong motion data set from buried explosions at the Nevada National Security Site (NNSS). The first experiment in a series (SPE1) was conducted in May of this year. It consisted of a 100 kg high explosive stemmed for coupling at 180 feet below the surface. In preparation for this experiment, predictive hydrodynamic calculations were performed, strong ground motion free-field and surface gauges were fielded, and a dense network of seismometers and some complimentary infrasound sensors were deployed. The data return for a majority of these sensors was excellent. This paper reports on a finite element analysis of the observable effects of an explosion in realistic earth material with particular focus on predicted and observed strong ground motion patterns. The model correctly incorporates the near-field cavity dynamics, energy deposition partitioned into internal (heat and plastic strain) and kinetic (e.g., radiated seismic) energy, giving more confidence in predicted free-field displacement/velocities and measured attenuation of the free-field peak velocity with distance. The degree of source asymmetry is studied with predictions of the hydrodynamic calculations for close-in free-field particle velocities. We present progress in improving our near-source modeling and predictive capabilities. A number of material test are presented on the granodiorite for both intact and weathered/damaged rock samples. These were used to improve our material model for the near-source environment. Additionally, a detailed 3D geologic framework model was created to represent the complex heterogeneities in the near-source environment (topography, faults, lithology, saturation and weathering). The improved material model was used in a set of 2D axially symmetric and a set of 3D simulations developed for simulating the Source Physics Experiment site. The site is dissected by two prominent faults. These faults have proven to control the radial asymmetry of the near field ground motion. Comparisons to the data provide ample information to study dry and water-saturated fractures, local lithology and topography on the radiated seismic wavefield. Spallation on SPE1 is predicted well by an empirical scaling relationship developed for nuclear explosions with nominal scaled depths of burial ($\sim 120 \text{ m/kt}^{1/3}$). This fact is astonishing considering that SPE1 is very over-buried $940 \text{ m/kt}^{1/3}$. This result is probably due to compensating effects of a low-porosity granite medium and a water table reaching almost to the free surface on Climax Stock. Nuclear tests on which the empirical relationship was based were overlain with ~ 640 meters of tuff with varying degrees of porosity which absorbs energy carried by shock waves. Estimates of bulk wave speeds in a weathered layer and in the basement rock where SPE1 was emplaced

15. SUBJECT TERMS

16. SECURITY CLASSIFICATION OF:

16. SECURITY CLASSIFICATION OF:			17. LIMITATION OF ABSTRACT	18. NUMBER OF PAGES	19a. NAME OF RESPONSIBLE PERSON
a. REPORT unclassified	b. ABSTRACT unclassified	c. THIS PAGE unclassified	Same as Report (SAR)	10	

OBJECTIVES

The National Center for Nuclear Security (NCNS) has chosen the Nevada National Security Site (NNSS) as the test location for the Source Physics Experiment (SPE-N) program. The intent of the SPE-N program is to provide data to improve strong ground motion prediction capabilities (ranging from coupled to decoupled scenarios) as well as seismic wave generation and propagation detection thresholds. Verification and validation of these models will then enhance our ability to detect and discriminate “low yield” nuclear explosions apart from conventional explosion tests and earthquake signals. NNSS was chosen as the test-bed for it provides an ideal natural laboratory for investigating the detection limits of our current suite of technologies. The geology at the NNSS is very well studied and the current infrastructure provides a unique facility where the U.S. has had extensive experience in nuclear and high explosive testing, and sensor development.

Our goal is to develop analytical and simulation capabilities that will provide a physical basis for modeling the important facets of explosion phenomena. The important components of our approach include 1) utilizing three-dimensional fully-coupled strong motion hydrodynamic codes that will allow us to explicitly model near-source finite displacement on faults as well as surface spall/slapdown (the gravitationally derived signal from lofted earth material) that is an important source of shear waves; 2) developing and implementing models that will allow us to realistically treat the microcrack releases that dominate near-source energy; 3) coupling the strong motion code to higher order spectral element codes with variable gridding to accurately model the effect of surface topography; 4) coupling our hydrodynamic calculations to seismic source models that utilize compensated linear vector dipole (CLVD) models in order to unequivocally separate source-generated shear waves from scattering-generated shear waves; and 5) using a coupled Eulerian-Lagrangian approach to model shots or shots near voids or rubble columns where the momentum transfer at the air-rock interface plays a crucial role in energy coupling, shock propagation, and permeability to radioactive gasses.

RESEARCH ACCOMPLISHED

The SPE-N is designed to provide a carefully controlled seismic and strong motion data set from buried explosions at the NNSS. The planned experiment series may have as many as nine individual high explosive tests.

The first experiment in the series was conducted in May of this year. It consisted of a 100 kg high explosive stemmed for coupling at 180 feet below the surface. In preparation for this experiment, predictive hydrodynamic calculations were performed, strong ground motion free-field and surface gauges were fielded, and a dense network of seismometers and some complimentary infrasound sensors were deployed. The data return for a majority of these sensors was excellent. We report below some of the advanced simulations and insights gained from the data analysis.

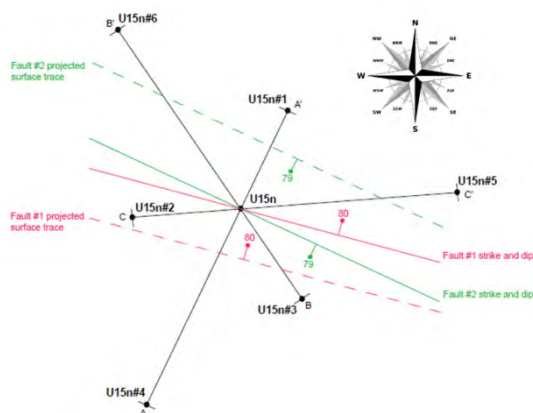


Figure 1. Top view of the general setup of the SPE1 experiment.

The first SPE-N high explosives (HE) experiment, SPE1, was placed in the U15n borehole in Area 15 of the Nevada National Security Site (NNSS). The borehole was drilled to a depth of 190 feet and stemmed up to place a canister of 100 kg of HE at 180 feet. Six monitoring boreholes were drilled at different azimuths to place free-field accelerometers (Figure 1). Two notable faults were seen in the U15n borehole while it was being drilled. There was no surface expression of the faults so they are mapped as inferred on Figure 1. The faults were steeply dipping and intercepted the U15n wellbore at 85 feet and 105 feet depth. Another unexpected curiosity was that U15n intercepted a perched water table at 70 feet which meant the granodiorite was saturated below this depth for SPE1.

1D Predictive Modeling. A series of 1D predictive calculations were performed before the first shot (SPE1) in order to provide acceleration ranges that gauge instruments would be subjected to. These calculations were

conducted utilizing LANL’s CASH hydrodynamics code. The material model for the granite medium is composed of an equation of state (EOS) combined with a strength model. The EOS was based on the one developed by Tillotson (1962) for the granite. This EOS is an analytical type and it introduces a dependency on the specific internal energy of the material, which makes it suitable to cover all the zones of the simulation. Also, the EOS accounts for solid-to-vapor phase changes (which does not typically happen in HE experiments, but is necessary for modeling nuclear explosions). The material model is completed by combining the EOS of the rock with an appropriate strength model. The strength model describes the resistance of the material to shear deformation. For rock-like materials, the shear strength is dependent on the confinement pressure. The main component of the strength model is the “yield surface”, which describes how the shear strength changes with the confinement pressure. The yield surface used in the current work was derived from the one proposed by Fossum and Brannon [2004]. Some modifications were introduced to the original yield surface in order to match the experimental data from the Piledriver and Hardhat events. The shear strength material model utilized also includes a damage model. The damage model relaxes the yield surface as a function of the equivalent plastic shear strain. At the beginning of the simulation the damage parameter is set to zero everywhere. As the simulation progresses and the material starts to yield in shear, the equivalent plastic shear strain increases. Complete damage was obtained when the plastic shear strain reached a value of 0.05.

In Table 1 and Table 2 the results for the radial velocity obtained from the 1D simulations for points located at 10 m and 20 m range are compared against the observed quantities. There is a quite noticeable dispersion of the observed peak radial velocity values for the 10 m range. The 1D numerical prediction is aligned with the peak velocity observed in the instrument U15n#2. A similar behavior is observed at the 20 m range. In this case the numerical results are in agreement with instrument U15n#6.

The 1D simulation is only a first order approximation and represents a coarse representation of the real emplacement of the experiment, i.e., no free surface effects are considered and no heterogeneity is taken into account in the computational model. However, it is known from surveys done at the test site that the shot point is “shielded” by two fault systems that would be expected to have an effect on the waveforms of the observed velocities. A clear example of this is shown in Figure 2 where it can be observed that all of the measuring points located at shot level are behind one of the fault systems, i.e. there is no clear direct path between the shot point and any of the instruments. The existence of these fault systems implies that any realistic computer modeling of the real world experiment must be done through a full 3D model which takes into account the full arrays of geological features, i.e., fault, fractures, topography, etc. Because of this, and in order to demonstrate the phenomenology effects arising when taking into account the real geologic structure, a series of 3D finite element simulations are reported in the next section.

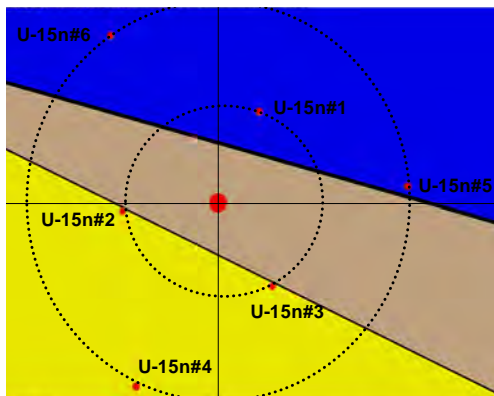


Figure 2. Top view at shot level. Position of instruments relative to shot point.

Table 1: Peak Radial velocity – 10 m range.

Station	Velocity (m/s)
1D Calculation	1.41
U15n#1	2.30
U15n#2	1.35
U15n#3	0.35

Table 2: Peak Radial velocity – 20 m range.

Station	Velocity (m/s)
1D Calculation	0.52
U15n#4	0.16
U15n#5	N/A
U15n#6	0.52

3D Phenomenological Modeling. LANL finite element simulations for the SPE1 shot included calculations using the coupled Euler-Lagrange capability of the Abaqus code (Abaqus/CEL). These simulations were accomplished by using an Euler region for the explosive charge and a Lagrange region of the geologic model.

The Euler region (Figure 3) was large enough to encompass the final deformed cavity caused by the charge. It included elements initially containing Jones-Wilkins-Lee (JWL) EOS for heavy ammonium nitrate fuel oil to form a sphere-equivalent volume for the cylindrical SPE1 explosive charge. The remaining elements, overlapping the rock region, were void at the start of the calculation.

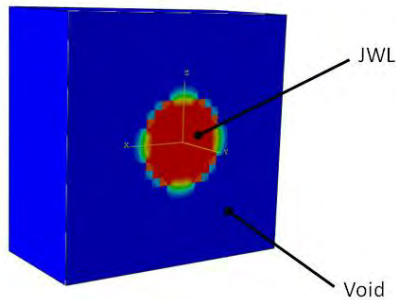


Figure 3. Eulerian region cut by xz -plane.

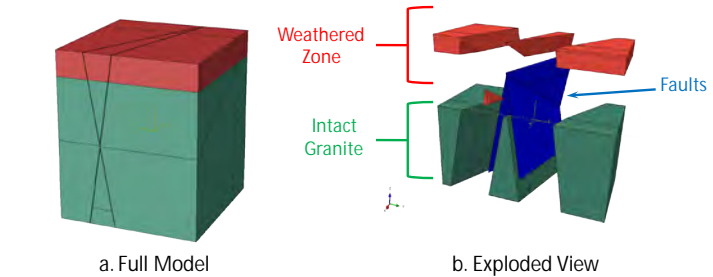


Figure 4. The 3D geologic framework model (GFM) for the Climax Stock site showing the Lagrangian regions used for the finite-element analysis.

LANL's GAMUT (Geologic Assessment Methodology for Underground Targets) process was used to create the geologic framework model (GFM) shown in Figure 4. This first-order GFM integrated a weathered granite layer over a half-space of intact granite bisected by the two major faults identified during the drilling of the emplacement hole. Each of these individual units and the faults were modeled explicitly in the Lagrange portion of the model. The blocks were modeled using continuum elements while the faults were handled as shell structures.

These calculations used material models for the rock based on properties provided above for use in the CASH simulations. However, the relevant constitutive models which have been validated for this site were not available as Abaqus user materials at the time that these calculations were performed, and native Abaqus constitutive models were used, include a Drucker-Prager yield surface combined with a linear U_s - U_p EOS with p - α compaction. Consequently, we do not propose that the calculations presented herein provide an accurate representation of the magnitude of the shock environment. However, our intent is to demonstrate possible phenomenology that could explain some anomalous measurements from this experiment.

Specifically, the described set-up, with faults included, allows the study of the effects of those faults on the local ground shock. For a spherical, or near-spherical (i.e., right circular cylinder with length-to-diameter of 1) we expect a spherical shock environment, with similar stress or motion histories at similar ranges from the shot; with perturbations in material causing insignificant differences in the measured response.

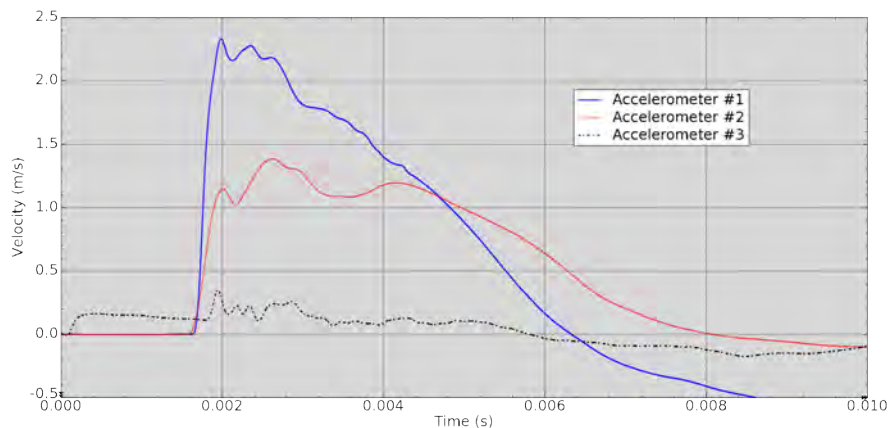


Figure 5. Radial velocity histories from accelerometers at the 10 m range.

However, as shown in Figure 5, the three radial velocities derived from the accelerometers at the 10-m range are quite different from one another. The differences, particularly the very low signal from accelerometer 3, could be due to a number of factors, including faulty gauge set-up, mis-orientation, or as we show below, their placement relative to the faults.

Figure 6 shows the location of the three 10-m range accelerometers at shot level. The figure includes the projection of the two faults at this elevation, illustrating that accelerometers 2 and 3 are on or very near to the thinner of the two faults. In fact, when applying an algorithm to find target nodes based on coordinates of a desired location, the node closest to accelerometer 2 was found to be on the fault while the node closest to accelerometer 3 was found to be on the edge of the block outside of the fault. This is simply fortuitous, and so the target node list was expanded to include companion nodes at both locations so that adjacent nodes on the interior block, on the fault, and on the exterior block were all saved for study.

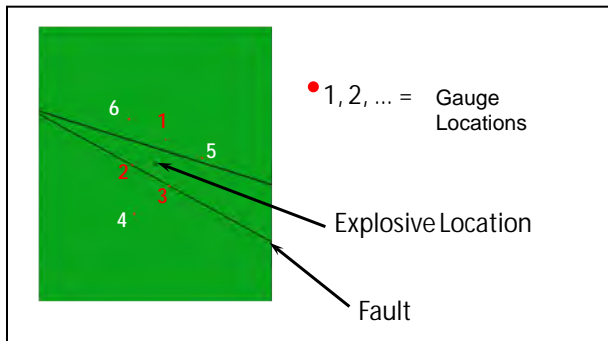


Figure 6. Geometry on horizontal plane through explosive center.

Histories for these locations are illustrated in Figure 7; Figure 7b representing accelerometer 2 and Figure 7c representing accelerometer 3. Two observations can be made from these plots. First, history pairs taken in each geologic unit – that is, the two histories in the interior block, the two histories in the fault, and the two histories in the exterior block – are nearly identical to each other. And second, the peak radial velocity for both the pair on the fault and for the pair on the exterior block is of the order of one-half the peak radial velocity of the pair on the interior block.

This suggests that if accelerometer 2 is actually located in the interior block and accelerometer 3 is actually located either on or outside of the fault, then the factor of two difference between these two measurements is consistent with the effects of the fault as observed in the calculation.

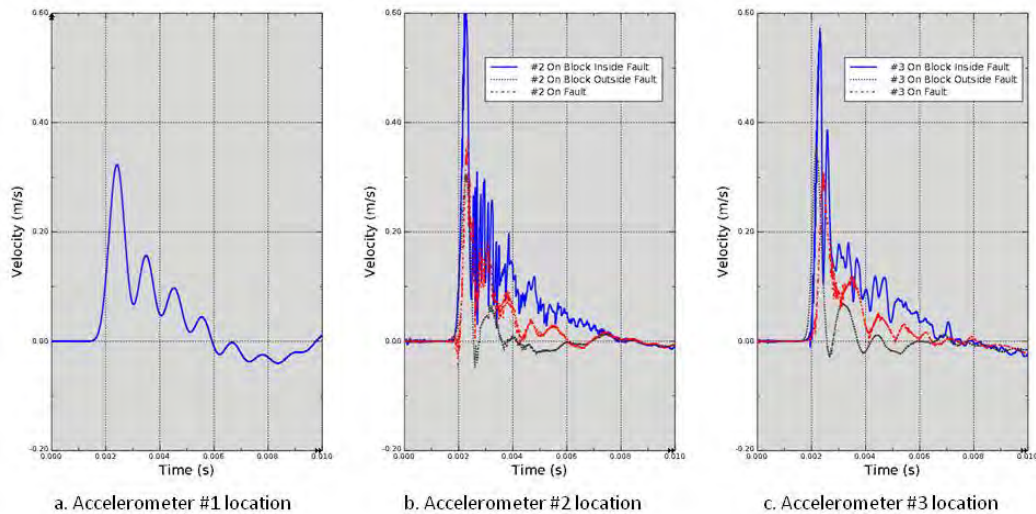


Figure 7. Velocity histories computed at the 10 m range.

Figure 7a illustrates the computed history for the location of accelerometer 1 in the block exterior to the wider of the two faults. Unlike the data, the computed history at this location is not significantly different in magnitude than those computed in the exterior block at accelerometer locations 2 and 3. This accelerometer might have produced faulty data. On the other hand, we understand from the drilling logs that the wider fault may have vuggy zones which could inhibit propagation of shock in the line of sight between the charge and the accelerometer, thus producing the lower motion.

The phenomenology described for accelerometers 2 and 3 is illustrated by review of snapshot plots of contours of pressure and velocity scalar magnitude. Figure 8 and Figure 9 respectively include contour plots of these variables on three planes through the charge. In both cases, plot “a” is the horizontal plane, plot “b” is the vertical east-west plane, and plot “c” is the vertical north-south plane. Each plot illustrates that the faults have a significant impact on the character of explosive energy propagation into the rock.

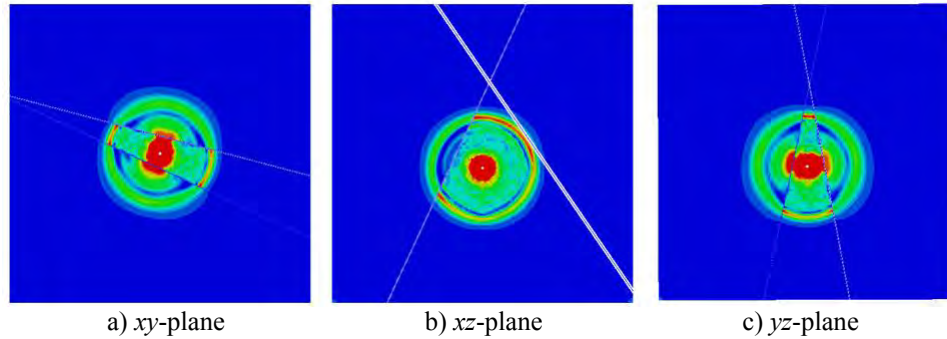


Figure 8. Pressure contours at 4 ms.

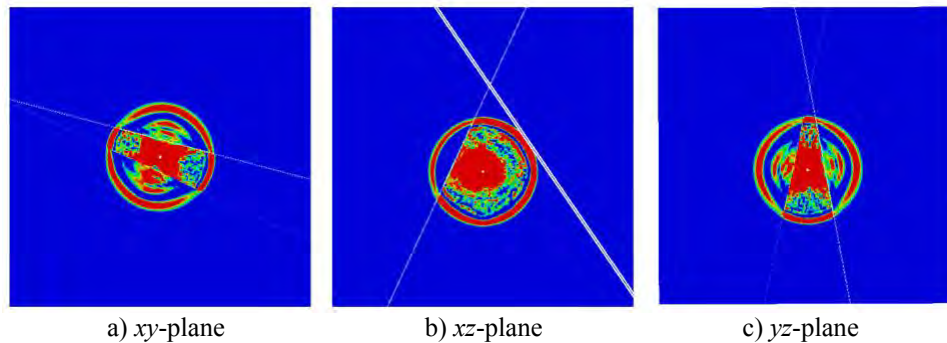


Figure 9. Scalar velocity magnitude contours at 4 ms.

The phenomenological model presented in this section will be improved by the incorporation of a proven material model for granodiorite medium developed by taking as a basis the Hardhat and Piledriver nuclear tests, Rougier et al. (2011). Results from the 3D simulations using this improved material model will be presented at the conference.

Spallation on SPE1. The Defense Threat Reduction Agency fielded accelerometers on the free surface over SPE1 at six sites emanating from ground zero. The stations were located at the wellhead and in steps of 10 m on a trajectory $\sim S26^\circ W$ out to a distance of 50 m. All recordings at all six sites indicated that accelerations reached or exceeded $-1g$ on the vertical components and showed a brief dwell time during which the instrument was in ballistic free flight. For spallation, the horizontal extinguishing distance r_{max} yield scales as

$$r_{max} = 475 W^{(0.26 \pm 0.03)} \quad (1)$$

in meters for nuclear explosions with $\sim 2 < W < \sim 1000$ kt below the water table on Pahute Mesa (Patton, 1990). This distance refers to where spallation is extinguished on the free surface. It scales approximately as the quarter-root of the yield.

For SPE1 (doubling its yield for nuclear equivalence, $2 \cdot 10^{-4}$ kt), r_{max} works out to be ~ 52 meters. This estimate involved a big extrapolation to a small yield chemical explosion in granite on Climax Stock. Nevertheless, it seems to have done a good job predicting that spall would be seen out to the most distant free-surface accelerometer on SPE1 (50 meters). What is surprising though is that this empirical-based formula was based on nuclear explosions with more or less normal emplacement depths, ~ 120 scaled meters, yet SPE1 was very over-buried, e.g., 940 scaled

meters. Under these circumstances, one would expect spall to be extinguished at shorter distances than the formula predicts and the observations showed.

This result raises questions about the medium-dependence of spallation since the explosions used for calibration were overlain with ~640 meters (the average standing water level on Pahute Mesa) of tuff with varying degrees of porosity. Porous media absorbs energy carried by shock waves, and perhaps the extinguishing distance would have been even greater on Pahute Mesa were it not for the porosity of the medium above the water table. The reason the r_{max} formula worked for SPE1 could be due to the compensating effects of a low-porosity medium and a water table reaching almost to the free surface. These conditions were present on SPE1 and at the Balapan test site in central Asia during nuclear testing years and for the Depth of Burial (DoB) experiments in 1997. The DoB chemical shot on 31Aug97 with a scaled DoB of 814 meters shows a ground-zero spall recording very similar to what is observed for SPE1 (see Figure 10). The comparison of GZ velocities is even more impressive.

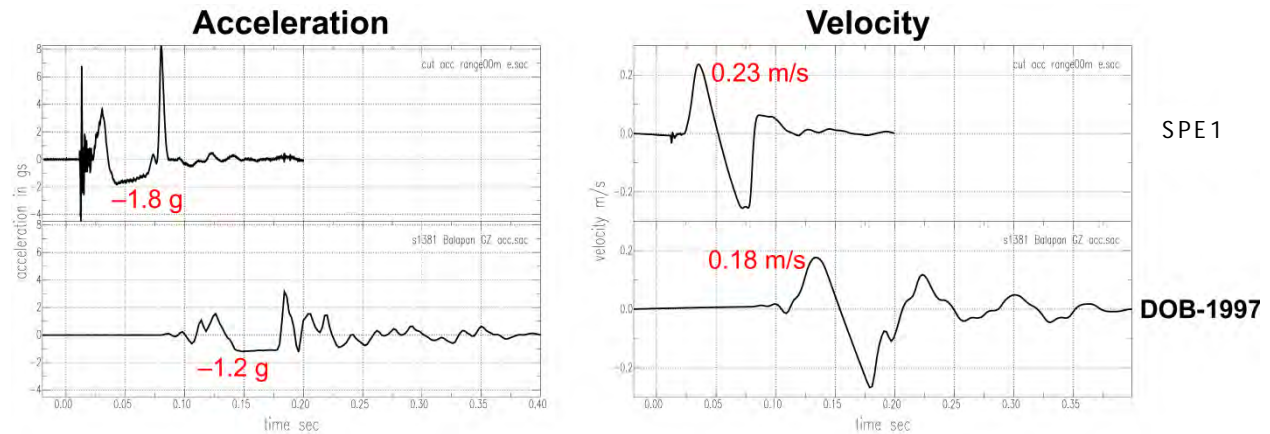


Figure 10. Velocity and acceleration waveforms for SPE1 test and for Balapan test of 31Aug97.

Analysis of travel time delays observed on free-surface accelerometers. Consider a simple Earth structure of a layer over a halfspace, where the layer represents the “weathered” granite near the free surface on Climax Stock, and the halfspace represents more competent granite in the upper 600 meters or so below the weathered layer. P wave speeds are assumed to be constant in both the layer and the halfspace. Let H_w be the thickness of the surface layer in meters, α_w be the bulk P wave speed in the layer in m/s, α_s be the bulk P wave speed in the halfspace, and tt_P be the travel time of P waves from the SPE1 point of detonation to a free surface accelerometer. The travel time was measured at an accelerometer on the free surface 10 m from ground zero. The slant-range is 55.77 m. Assuming straight rays in the halfspace and vertical propagation through the layer, an approximate equation for tt_P is $H_w/\alpha_w + (55.77 - H_w)/\alpha_s$. The measured travel time is 0.0218 s. Table 3 provides estimates of α_w for various H_w values while holding α_s fixed at 5500 m/s. Table 4 provides estimates of α_w for various α_s values while holding H_w fixed at 30 m. Shear wave speeds β_w and β_s are also provided assuming a Poisson ratio ν of 0.23 in the layer and the halfspace.

Table 3: $\alpha_s, \beta_s = 5500, 3258$ m/s and $\nu = 0.23$

Model #	H_w (m)	α_w (m/s)	β_w (m/s)
1	35	1942	1151
2	30	1753	1039
3	25	1543	914
	20	1308	775
5	15	1043	618
6	10	742	440

Table 4: $H_w = 30$ m and $\nu = 0.23$

Model #	α_s (m/s)	β_s (m/s)	α_w (m/s)	β_w (m/s)
2	5500	3258	1753	1039
12	5000	2962	1802	1068
22	4700	2785	1839	1089

Note that wave speeds in the layer are a strong function of layer thickness (Table 3), but are insensitive to wave speeds in the halfspace (Table 4) for a constant layer thickness. To discriminate between these models, we must resort to other measurements.

Analysis of *Rg* dispersion recorded on geophone Lines Nos. 1 and 2. The short-period Rayleigh wave *Rg* is sensitive to shallow Earth structures and is excited very well by shallow sources like explosions. In uniform structures it propagates to regional distances (~200 km and more) as a Airy phase near 1 Hz, i.e., does not show dispersion like normal surface waves do. At higher frequencies (> ~5 Hz), *Rg* waves are dispersed, and the dispersion characteristics provide information about Earth structures. The horizontal wavelength λ_H equals $C \cdot T$, where C is phase velocity and T is period in seconds. As a rule of thumb, the depth of penetration into the Earth of surface waves is about one third λ_H , and the waves are sensitive to the integrated effects of structures above this depth. For example, a 5 Hz *Rg* wave with phase velocity 2000 m/s has λ_H equal to 400 m and a depth of penetration of ~133 m. So *Rg* waves with frequencies greater than ~5 Hz provide useful information about structures shallower than ~100 m.

Figure 11 shows a perspective of geophone Lines 1 and 2 which are located entirely in the granite body of Climax Stock. Line 1 trends N4°W, while Line 2 trends N49°E. Topographic relief is 210 m on Line 1 while it is only 30 m on Line 2. Each profile consists of 20 stations, starting at an offset 100m from ground zero, and sampling range at 100 m increments. The sensors are 4.5 Hz geophones, and *Rg* waves from SPE1 were recorded on the vertical-component channels. Figure 12 shows a seismic record section for Line 2 in two frequency bands, the one on the left for the full bandwidth after correcting for instrument response, the one on the right for 5-Hz low-pass filtered records. The records are proportional to ground velocity. The latter profile clearly shows *Rg* waves, while the former is dominated by *P* wave arrivals. The red lines indicate apparent phase velocity for both wave types, phase velocity because they mark the same “phase”: i.e., for *P* waves, the “first-motion break” and for *Rg* waves, the same “zero-crossing” on the waveform as the wave moves out. Because of the effects of attenuation, especially at high frequencies, it is better to measure surface-wave phase velocity through narrowband filters.

Measurements of *Rg* phase velocity are shown in Figure 13 along with predicted dispersion curves for selected velocity models in Table 3 and Table 4. The measurements are shown as horizontal bars because the frequency varies somewhat along the profile in spite of the narrowband filters used. The black bars are for Line 1, the red bars are for Line 2. Two red bars are shown for the 10-12 Hz band, one for a filter designed with corners between 7.5 and 15 Hz, and the other for a filter designed with corners between 10 and 20 Hz. The latter filter gave a result with better frequency resolution, and it is the preferred measurement. The dispersion curves for both profiles are similar, but *Rg* waves are slightly faster on Line 1. The reason for this could be related to the average thickness of the weathered layer (greater thickness on Line 2), or it could be related to averaged wave speeds in the upper 200 m (slower on Line 2, perhaps because Line 2 traverses pre-conditioned Earth structures from Hardhat and Piledriver tests in the 1960s). None of the predicted dispersion curves in Figure 13a for three velocity models (#2, 4, and 6) from Table 3 fit the observations. Indeed, the layer would have to be unreasonably thick to obtain a match for a halfspace with a *P* wave speed of 5500 m/s. Nevertheless, the shape of the phase velocity dispersion curve is fit better by structures with a thick layer than with a thin layer. Figure 13b shows dispersion predictions for three models with a fixed layer thickness of 30 m while *P* wave speed of the halfspace is reduced from 5500 to 5000 to 4700 m/s (models # 2, 12, and 22 in Table 4). Model 22 fits the dispersion curve for Line 1 fairly well, while a slight increase in layer thickness and/or a reduction in velocities would be needed to improve the fit of model 22 to Line 2. Note that a *P* wave speed of 4700 m/s in the halfspace is in excellent agreement with apparent phase velocities of *P* wave first motions observed on Lines Nos. 1 and 2.

In summary, *P* wave travel times and *Rg* dispersion curves provide complementary information enabling the bulk wave speeds to be estimated in the top 200 m of Climax Stock using SPE1 measurements off a free-surface accelerometer and two geophone profiles. These estimates suggest that the speeds are much lower than the velocities determined from borehole geophysical logs reported by Broome and Pfeifle (2011) for the emplacement hole U15n.

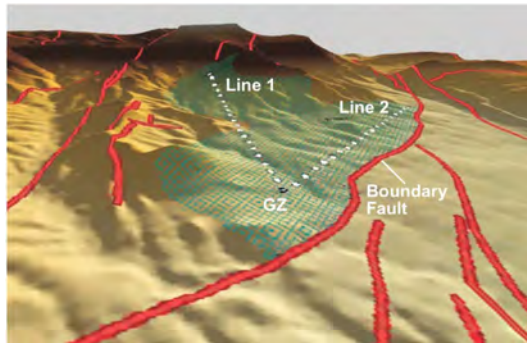


Figure 11. SPE1 geophone lines 1 and 2 on Climax Stock granite.

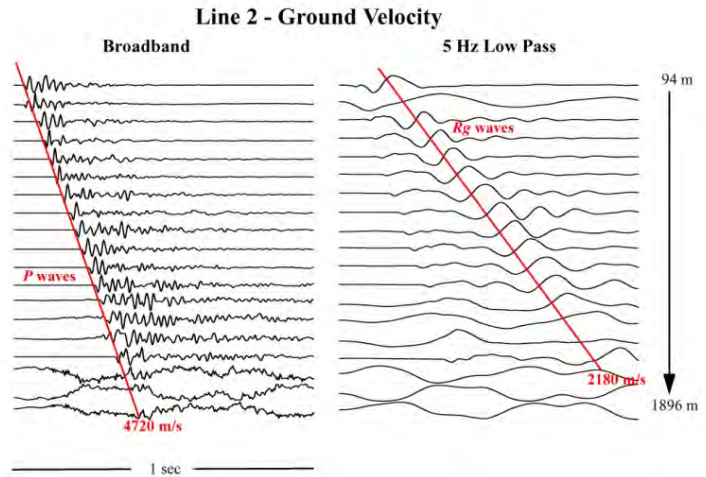


Figure 12. Line 2 instrument-corrected velocity waveforms.

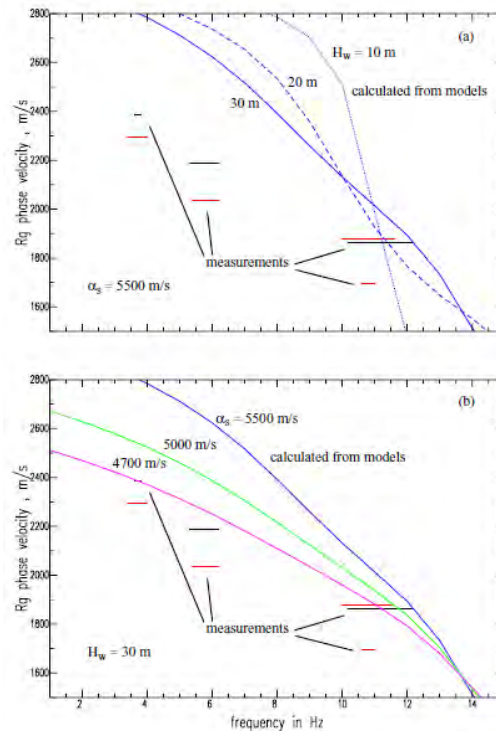


Figure 13. R_g dispersion curves, measured and models.

a) Predictions holding α_s fixed, varying H_w . b) Predictions holding H_w fixed, varying α_s .

CONCLUSIONS AND RECOMMENDATIONS

Based on the results discussed above we draw the following conclusion from this study:

1. Hydrodynamic Calculations: Faults (and Joints) Matter
 - a. Radiation pattern is controlled by the faults in both the magnitude and anisotropy of the shock and seismic propagation.
 - b. Validation results show much stronger granite in the near-field. New hardening models for the granite show a better match to nuclear test data and will hopefully improve our match to future shots SPE2 and SPE3.

2011 Monitoring Research Review: Ground-Based Nuclear Explosion Monitoring Technologies

- c. Complex wave field brings into question some of the free field accelerometer data but shows need for improved understanding of gouge vs. fluid filled faults (joints).
2. Seismic Analysis
 - a. Estimates of bulk wave speeds in a weathered layer and in the basement rock where SPE1 was emplaced were obtained from P travel times and Rg dispersion curves. These speeds are considerably lower than those determined from core samples, indicating a length scale dependence of material properties.
 - b. Judging from ground zero acceleration records, spall phenomena on SPE1 and on the 31 August 1997 Depth of Burial shot at the Balapan test site in central Asia are quite similar.
 - c. The lateral extent of spall on SPE1 is well predicted by an empirical scaling relationship for Pahute Mesa explosions with nominal scaled depths of burial, a surprising result since SPE1 is very over-buried ($\sim 940 \text{ m/kt}^{1/3}$). This raises questions about material dependences since Pahute Mesa shots were overlain with tuff of varying degrees of dry porosity while SPE1 was fire in granite of low porosity and a water table reaching nearly to the surface.
 - d. The apparent attenuation of Rg waves on Line 2 is similar to what was observed at the Balapan test site where effective Q values are very low. Amplitude behavior on Line 1 is unconventional, showing an increase in Rg amplitudes after a square-root of “ r ” distance correction for surface-wave spreading. This behavior suggests non-uniform geometrical spreading or an effect of non-planar sub-surface earth structures.

We recommend continued modeling of future events using Abaqus/CEL. This modeling will incorporate into Abaqus the advanced constitutive models being developed at LANL. Moreover, Abaqus/CEL is capable of explicit modeling of various aspects of test design, such as the placement hole and stemming, and these should be included in future simulations as well.

ACKNOWLEDGEMENTS

The authors would like to thank the National Nuclear Security Administration and the National Center for Nuclear Security for sponsoring this research effort. Large field activities like the Source Physics Experiment require the cooperation of individuals from many organizations. Thanks to our colleagues and collaborators for their support and the advice provided during this project.

REFERENCES

- Broome, S. and T. Pfeifle (2011). Phase 1 mechanical testing results on core from borehole U-15n, Nevada National Security Site, in support of NCNS Source Physics Experiment, Sandia National Laboratory Memorandum dated 8 June 2011.
- Fossum A. F. and R. M. Brannon (2004). THE SANDIA GEOMODEL: Theory and User's Guide. Sandia National Laboratories.
- Patton, H. J. (1990). Characterization of spall from observed strong motions on Pahute Mesa, *Bull. Seismol. Soc. Am.* 80: 1326–1345.
- Rougier, E., C. R. Bradley, H. J. Patton and E. E. Knight (2011). Yield and depth of burial hydrodynamic calculations in granodiorite: implications for the North Korean Test Site, these Proceedings.
- Tillotson, J. H. (1962). Metallic equation of state for hypervelocity impact, AF 29(601)-4759, ARPA Order 251-61.
- Yang, X. and J. L. Bonner (2009). Characteristics of chemical explosive sources from time-dependent moment tensors, *Bull. Seismol. Soc. Am.* 99: 1, 36–51.